frontiers | Frontiers in Mechanical Engineering

TYPE Original Research
PUBLISHED 07 January 2026
DOI 10.3389/fmech.2025.1715466

OPEN ACCESS

EDITED BY
Chengxi Zhang,
Jiangnan University, China

REVIEWED BY
Tianle Yin,
Jiangnan University, China
Chenglong Xu,
First Affiliated Hospital of Sun Yat-sen University, China
Bo Hu,
Nankai University, China
Lanhao Zhao,
Beijing University of Technology, China

*CORRESPONDENCE
Yuping Li,
liyuping19920220@163.com

RECEIVED 29 September 2025
REVISED 09 December 2025
ACCEPTED 15 December 2025
PUBLISHED 07 January 2026

CITATION
Zhang Y and Li Y (2026) Motor automation speed regulation method with sliding mode control and adaptive gain.
Front. Mech. Eng. 11:1715466.
doi: 10.3389/fmech.2025.1715466

Motor automation speed regulation method with sliding mode control and adaptive gain

Yu Zhang[1] and Yuping Li[2]*

[1]School of Engineering, Zhengzhou Technology and Business University, Zhengzhou, China, [2]School of Mathematics and Statistics, North China University of Water Resources and Electric Power, Zhengzhou, China

Introduction: Motor speed control is crucial for maintaining the normal operation of motors. In view of the limitations of current motor speed control methods, such as high parameter dependence, obvious control signal buffering, and low flexibility, an automatic speed control model combining Sliding Mode Control and adaptive gain is proposed.
Methods: This model combines adaptive gain with a Sliding Mode Control to design an Adaptive Sliding Mode Control for motor speed control. Then, the super helix algorithm is used to adjust the sliding mode gain coefficient to suppress the controller's buffing problem. At the same time, an evaporation constant is introduced to improve the particle swarm optimization algorithm, and the controller parameters are optimized using the improved particle swarm algorithm to enhance the model's stability and achieve automatic speed regulation of the motor.
Results: In the dynamic experiment, it was proposed that the current fluctuation of the model was always kept within $\pm$0.10A, demonstrating high stability. In addition, the research proposes that the maximum speed estimation error of the model is 5.77%, which is superior to the error calculation results of the comparison models and far less than the standard requirement of 8.00%.
Discussion: The model proposed in this study exhibits superior speed regulation performance, achieving high stability, low vibration, and strong robustness in motor automatic speed regulation control. It can better meet the speed control requirements in the field of motors, thereby better ensuring the safe operation of the motor.

KEYWORDS

adaptive gain, motor, PSO, sliding mode control, super-twisting algorithm

1 Introduction

Motors can convert electrical energy into mechanical energy according to the law of electromagnetic induction. They are the core power source in manufacturing and play a vital role in modern industry (Mapui et al., 2025). Motor control systems are multivariable and nonlinear, and they are easily affected by speed fluctuations, which cause performance decline and even failure (Cheng et al., 2025). In this context, automatic motor speed regulation becomes an important topic in the field of motor control. The primary approaches to automatic speed regulation include scalar control, direct torque control, and vector-based control. Scalar control exhibits limited robustness against disturbances, whereas direct torque control suffers from torque ripples. Neither can meet the requirements of the current automatic motor speed regulation (Li et al., 2025). Vector

control decouples the torque and flux components of the motor, thereby improving dynamic response and providing high control efficiency and anti-interference performance (Ge and Wang, 2025). Sliding Mode Control (SMC) is a classical vector control method that effectively suppresses external disturbance and internal parameter fluctuation in motor operation. It is simple in structure, efficient in operation, and robust (Zaghba et al., 2025). Particle Swarm Optimization (PSO) is a heuristic optimization algorithm that simulates the cooperative behavior of bird flocks to optimize parameters, providing strong global search ability (Deng et al., 2025). Adaptive gain is a parameter adjustment technique that dynamically adjusts system gain parameters to optimize control performance (Bao et al., 2024). Based on this, the study employs a SMC method for motor speed regulation, utilizing an adaptive gain design for the SMC. The Super-Twisting Algorithm (STA) is applied to suppress controller chatter, while an improved Particle Swarm Optimization (PSO) algorithm optimizes controller parameters. This ultimately establishes an automated motor speed control model. The innovative model integrates adaptive gain with SMC to design the controller, employing STA and an enhanced PSO algorithm based on evaporation constants to refine controller parameters, thereby improving control performance and providing a more efficient solution for motor speed regulation. It is anticipated that this model will enable more precise and efficient motor speed control, ensuring optimal motor operation.

The study's contributions are twofold: First, it introduces a controller with adaptive gain, which overcomes quality limitations in traditional speed regulation by enhancing the STA algorithm. Second, it establishes a motor speed control model that integrates multiple algorithms, including the improved PSO and STA algorithms, thereby significantly improving control performance. These advancements offer a more efficient and accurate solution for electronic speed regulation systems.

2 Related works

SMC is a control method with strong robustness and is widely applied in multiple fields such as robotics, automotive engineering, and power systems. For a long time, many scholars at home and abroad have conducted research on this. Huang H et al. proposed an actuator vibration suppression model based on an echo state network and SMC to enhance the performance of underwater flexible actuators. They designed a full-order SMC for vibration suppression and improved the system stability through proportional-differential control methods. However, there is still a deficiency in flexibility (Huang et al., 2025). To enhance the stability of wind power generation systems, Musarrat M N and colleagues proposed a fault-ride-through model based on SMC. By integrating SMC with a designed disturbance observer, they achieved effective control of DC link voltage and converter load disturbances. However, the dynamic adjustment mechanism for event-triggering thresholds remains imperfect, potentially affecting control performance under extreme conditions (Musarrat et al., 2024). To address trajectory tracking in underactuated nonlinear dynamic systems, Liu M. et al. proposed an SMC-based model. They designed an adaptive model with self-adaptive gain coefficients to compensate for fault disturbances, though the model still lacks sufficient dynamic adjustment capability (Liu M. et al., 2025). Scholars such as Liu Z proposed a tracking control model based on a fuzzy-feature-selection neural network and SMC to improve the tracking performance of bidirectional DC converters. Tracking control was achieved using a non-singular fast terminal SMC, and the controller parameters were optimized using a fuzzy neural network, thereby improving accuracy and stability. However, the model's dynamic speed regulation effect remains insufficient (Liu Z. et al., 2025). Hill J and other scholars, in order to improve the anti-interference ability of pitch motion of micro aircraft, proposed a vibration suppression model based on adaptive discrete-time SMC. By designing and improving the SMC, the flapping-wing micro-aircraft model was converted from continuous to discrete time for vibration suppression, thereby improving stability. However, it has a relatively high computational complexity (Hill et al., 2025).

Motor speed control is crucial to the regular operation of motors, and many scholars have conducted research on this topic. To improve the stability of the speed control system of permanent magnet synchronous motors, Jiang J et al. studied and proposed a speed control model based on non-singular fast terminal SMC. The sliding membrane surface was calculated by combining nonlinear functions with linear functions, and the stability of the control system was improved through the disturbance observer (Jiang et al., 2024). Yang H and other scholars have studied and proposed a speed control model based on synchronous space vector modulation for the problem of motor speed control. Closed-loop control is carried out through the synchronous space vector modulation method, and phase synchronization and current regulation are accomplished through the proportional-integral controller, thereby achieving rapid phase synchronization. However, it still has limitations in terms of adaptive adjustment ability and dynamic response speed (Yang et al., 2025). In order to conduct motor speed tracking control more efficiently, scholars such as Chen Z have studied and proposed a motor speed regulation model based on the synchronous prediction equation. The synchronous prediction of speed and current is carried out through the Taylor synchronous prediction equation, and the cost is evaluated through the quadratic cost function, which improves the control performance. However, the accuracy of this model highly depends on the system parameters (Chen et al., 2023). Scholars such as Rauth S S have studied and proposed a speed control model based on a stator voltage controller for the speed control problem of doubly-fed induction generators. By referring to the adaptive system and the improved decoupled stator voltage controller for grid synchronous control, and conducting rotor speed estimation, adaptive adjustment can be carried out relatively accurately. However, the chattering suppression effect on the controller is relatively insufficient (Rauth et al., 2024). To improve the accuracy of speed estimation in the sensorless vector control system of permanent magnet fine-tuning wheel-side drive motors, scholars such as Zhao T proposed a speed regulation control model based on fuzzy control. The speed estimation was carried out through the full-order current observer, and the fuzzy control algorithm and the superhelix algorithm were introduced to optimize the observer, which improved the control

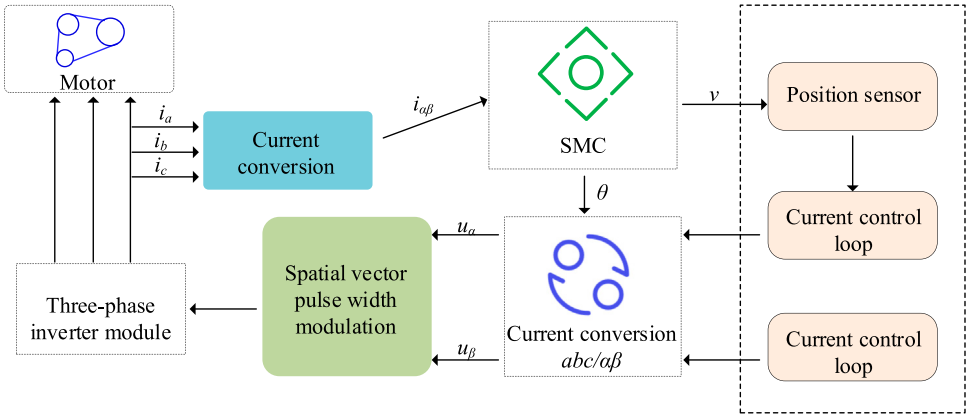

FIGURE 1
Motor speed regulation process based on SMC.

accuracy. However, the problem of the controller's excessive reliance on parameter Settings has still not been solved (Zhao et al., 2025).

In summary, current research on motor speed control primarily employs vector control for speed estimation, which improves control accuracy. However, relying solely on vector control for speed regulation not only over-relies on parameter settings but also tends to generate chattering, causing high-frequency oscillations in control signals. This makes it difficult to adapt to complex and variable operating environments, resulting in limitations such as poor robustness and low flexibility. To enhance the model's control performance, flexibility, and anti-interference capabilities, this study proposes a speed regulation model based on SMC and the STA algorithm. The goal is to improve the efficiency and accuracy of motor speed control, ensuring safe and efficient operation of the motor.

3 Speed regulation control model design based on SMC and STA

3.1 Controller improvement with adaptive gain

The motor consists of a stator, rotor, bearing, and other parts. The rotor is the component that controls the motor's load rotation. Rotor speed regulation is an important step in motor operation control. By adjusting different speeds, motor overload and wear can be effectively avoided (Zhang et al., 2023). SMC is a nonlinear control approach that regulates the system state by constructing a sliding mode surface and calculating the corresponding control rate. It has the advantage of efficient computation. In addition, SMC is highly insensitive to system parameter changes and external disturbances, which allows more stable control of the system state (Fang et al., 2023). Based on this, the study designs a controller to regulate motor speed. The motor speed regulation process is shown in Figure 1.

As shown in Figure 1, the motor speed regulation process based on SMC first transmits motor state information and position information to the current conversion module through position and current sensors to complete data conversion. The information is then transmitted to the space vector PWM unit to produce modulation signals, which are subsequently fed into the three-phase inverter for processing. Finally, information from the position sensor and inverter is input to the controller to control motor speed. In the SMC, the sliding mode surface and SMC rate are calculated and combined with the motor voltage equation to estimate motor position and control speed. The mathematical expression of the sliding mode surface is shown in Equation 1.

$$S = \begin{bmatrix} S_\alpha \\ S_\beta \end{bmatrix} = \begin{bmatrix} \tilde{i}_\alpha - i_\alpha \\ \tilde{i}_\beta - i_\beta \end{bmatrix} \tag{1}$$

In Equation 1, S_α and S_β denote the two components of the synovial surface function in the α-β static coordinate system, corresponding to the α-axis and β-axis, respectively. i_α and i_β are the actual measured values of the stator current in α and β axes respectively, $\tilde{i}_\alpha = \hat{i}_\alpha - i_\alpha$, $\tilde{i}_\beta = \hat{i}_\beta - i_\beta$, $\hat{i}_\alpha$ and $\hat{i}_\beta$ are the estimated values of the stator current in α and β axes respectively.

Based on these, the SMC rate is designed for input control. The mathematical expression of the SMC rate is shown in Equation 2.

$$\begin{bmatrix} V_\alpha \\ V_\beta \end{bmatrix} = K \begin{bmatrix} \hat{i}_\alpha \mathrm{sgn}\left(\hat{i}_\alpha - i_\alpha\right) \\ \hat{i}_\beta \mathrm{sgn}\left(\hat{i}_\beta - i_\beta\right) \end{bmatrix} \tag{2}$$

In Equation 2, sgn (.) represents the switching function, and K represents the gain coefficient.

The definition of the gain coefficient determines the stability of SMC. K is defined as shown in Equation 3.

$$K > MAX\left\{-R\left|\tilde{i}_\alpha\right| + E_\alpha \,\mathrm{sgn}\left(\tilde{i}_\alpha\right), -R\left|\tilde{i}_\beta\right| + E_\alpha \,\mathrm{sgn}\left(\tilde{i}_\beta\right)\right\} \tag{3}$$

In Equation 3, E_α represents back electromotive force. Using the computed sliding mode surface and SMC rate, the controller is designed for motor speed regulation. The working process of the controller is shown in Figure 2.

As shown in Figure 2, the sliding mode surface is designed based on input information, and the SMC rate is calculated to control the system state. The information is then fed into a low-pass filter to reduce chattering. According to the controller's design, it can

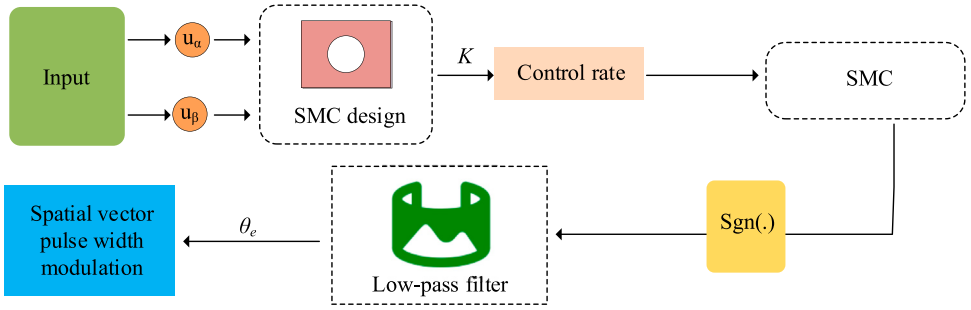

FIGURE 2
Working process of SMC.

achieve relatively stable speed control. However, due to the switching characteristics of SMC, chattering easily occurs. Smoothing with a low-pass filter can cause phase lag, which is difficult to meet the requirements of automatic motor speed regulation. To reduce chattering, the study replaces the sign function sgn(x) with a continuous and differentiable Sigmoid function for smoothing. The definition of the Sigmoid function is shown in Equation 4.

$$sig(x) = \left(\frac{2}{1+e^{-ax}} - 1\right) \tag{4}$$

In Equation 4, e represents the base of the natural logarithm, and a controls the slope variation.

Substituting the original function with a Sigmoid-based continuous switching approach mitigates chattering to some extent, but it does not eliminate the phase lag issue. Adaptive gain is a classical parameter tuning technique that enhances system dynamic response speed by dynamically adjusting gain parameters. To address phase lag and improve controller responsiveness, this study proposes an adaptive gain-based improvement for the SMC to boost stability. The adaptive filter is designed using adaptive gain coefficients to eliminate higher-order harmonics and suppress chatter. The mathematical expression of the adaptive filter is presented in Equation 5.

$$\begin{cases} \hat{e}_\alpha{}' = -\hat{\omega}\hat{e}_\beta - k_e(\hat{e}_\alpha - e_\alpha) \\ \hat{e}_\beta{}' = -\hat{\omega}\hat{e}_\alpha - k_e(\hat{e}_\beta - e_\beta) \end{cases} \tag{5}$$

In Equation 5, k_e represents the adaptive gain coefficient, and e_α and e_β represent back electromotive force.

In order to ensure the stable operation of the filter, the stability analysis is usually carried out by using the Lyapunov function, so that the filter can satisfy the stability theorem. The definition of the Lyapunov function is given in Equation 6.

$$V = \frac{1}{2}\left(\tilde{e_\alpha}^2 + \tilde{e_\beta}^2 + \tilde{\omega_r}^2\right) \tag{6}$$

In Equation 6, ω_r usually represents the motor equivalent electrical angular velocity. It changes little and is usually set to 0. When the derivative of V is negative, the model is stable. Taking the derivative of V in combination with Equation 5, the result of the derivative is shown in Equation 7.

$$V' = -k_e\left(\tilde{e_\alpha}^2 + \tilde{e_\beta}^2\right) - \tilde{\omega_r}\left(\hat{e}_\beta\tilde{e_\alpha} - \hat{e}_\alpha\tilde{e_\beta}\right) + \tilde{\omega_r}\tilde{\omega_r}' = V_1 + V_2 + V_3 \tag{7}$$

As can be seen from the result of the derivative, when a is large enough, V_1 is always negative, so as long as $V_2 + V_3 = 0$ is satisfied, V' can be set as negative. The adaptive law is set to satisfy the stability theorem. The adaptive law is defined as shown in Equation 8.

$$\hat{\omega}' = \hat{e}_\beta\tilde{e_\alpha} - \hat{e}_\alpha\tilde{e_\beta} \tag{8}$$

Based on adaptive gain and adaptive law, the SMC is improved to design the Adaptive Sliding Mode Control (ASMC) to enhance controller performance. The speed regulation process of ASMC is shown in Figure 3.

In Figure 3, the adaptive controller's speed regulation process first constructs the sliding mode surface based on the input signals and computes the SMC rate using the system state and a continuously differentiable Sigmoid-based smoothing function to ensure signal continuity. Then, the information is input to the adaptive filter and smoothed using an adaptive gain coefficient and an adaptive law to eliminate high-order harmonic interference and suppress chattering. The processed information is then sent through the space vector pulse width modulation stage to generate modulation signals, which are finally input to the inverter to convert them into a form suitable for driving the motor for automatic speed regulation.

3.2 Construction of an automatic speed regulation model based on STA and EC-PSO

This study has improved the control performance by using an ASMC controller to control the motor speed automatically, but the motor still tends to run at high speed, and the phenomenon of vibration occurs, which affects the control performance of the model. STA is a second-order SMC method. By adjusting the convergence coefficient and sliding mode surface coefficient, it reduces system chattering while improving control accuracy. Based on this, the study applies STA to improve ASMC to complete automatic speed regulation more accurately and efficiently. In STA, the SMC rate is calculated by adjusting the sliding mode gain coefficient for motor speed regulation. The

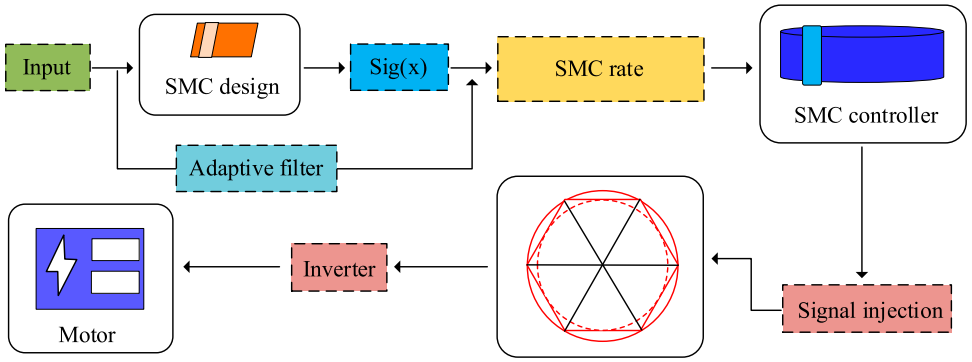

FIGURE 3
Speed regulation process of ASMC.

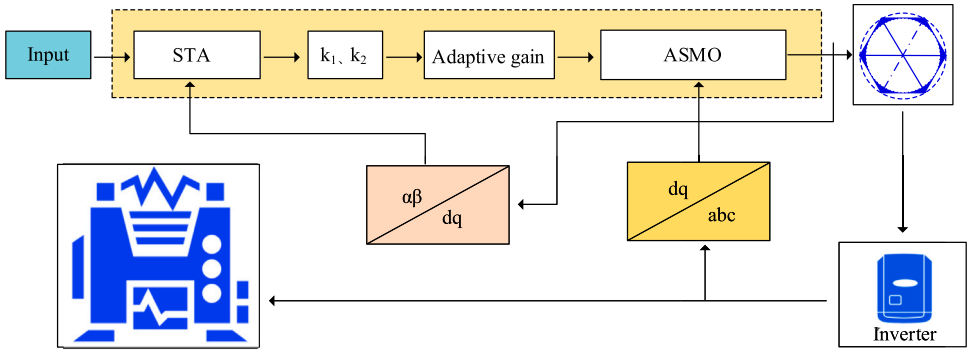

FIGURE 4
Working process of STA-ASMC.

definition of SMC coefficient in STA is shown in Equation 9; (Geromel et al., 2024).

$$\begin{cases} k_1 > 2\delta_1 \\ k_2 > k_1\left(5\delta_1 k_1 + 4{\delta_1}^2\right)/2\left(k_1 - 2\delta_1\right) \end{cases} \tag{9}$$

In Equation 9, k_1 and k_2 represent sliding mode gain coefficients, both greater than 0, and δ_1 is a normal constant, the critical value of the gain coefficient of the SMC is used to balance the convergence speed and the chattering amplitude of the controller, and to ensure that the system satisfies the arrival condition of the SMC.

Based on the adjustment of sliding mode gain coefficients by STA, the SMC rate is calculated as shown in Equation 10.

$$\begin{bmatrix} V_\alpha \\ V_\beta \end{bmatrix} = \begin{bmatrix} k_1\left|\tilde{i}_\alpha\right|^{\frac{1}{2}} sign\left(\tilde{i}_\alpha\right) + \int k_2 sign\left(\tilde{i}_\alpha\right) dt \\ k_1\left|\tilde{i}_\beta\right|^{\frac{1}{2}} sign\left(\tilde{i}_\beta\right) + \int k_2 sign\left(\tilde{i}_\beta\right) dt \end{bmatrix} \tag{10}$$

In Equation 10, $\tilde{i}_\alpha$ and $\tilde{i}_\beta$ represent estimated stator current, and $sign(.)$ represents the sign function.

By adjusting the SMC rate through STA, ASMC is improved to obtain the STA-ASMC speed regulation controller for more precise speed control. The working process of STA-ASMC is shown in Figure 4.

As shown in Figure 4, the STA-ASMC working process first inputs information into the STA layer and calculates the SMC rate using a fixed sliding mode gain coefficient. Then, in the adaptive controller, the Sigmoid function improves the switching function, and an adaptive filter is designed using adaptive gain to smooth the information and eliminate interference from high-order harmonics. STA improves ASMC and enhances accuracy, but STA-ASMC relies heavily on parameter tuning and may increase chattering at high motor speeds. The PSO algorithm is a widely used parameter optimization method renowned for its robust global search capabilities. While other meta-heuristics like genetic algorithms and ant colony optimization rely heavily on fixed parameters such as crossover rates, mutation rates, and pheromone dissipation coefficients—showing limited flexibility in dynamic adjustments and struggling with complex nonlinear optimization problems—PSO stands out with fewer parameters. By dynamically adjusting particle positions and velocities through inertia weights, PSO effectively tackles nonlinear optimization challenges. Compared to genetic algorithms and other meta-heuristics, PSO demonstrates superior flexibility, computational efficiency, and robust performance in such scenarios. Based on this, the study applies PSO to tune STA-ASMC parameters to improve controller performance. In PSO, the optimal parameters are solved by comparing and updating individual best values and global best

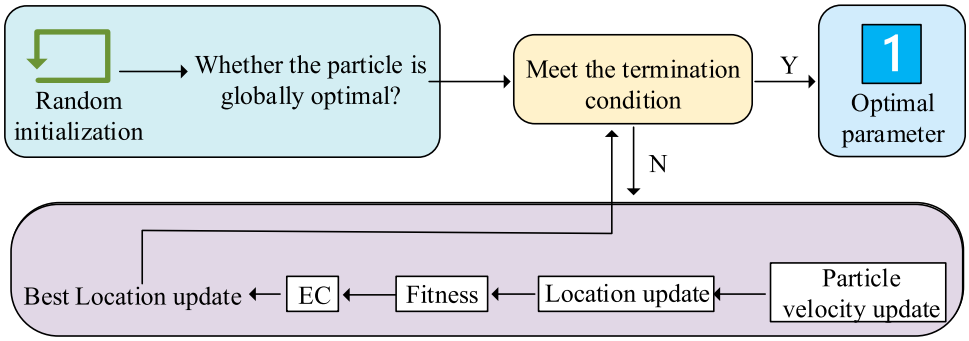

FIGURE 5
Working process of EC-PSO algorithm.

values. The update of particle velocity is mainly achieved by modifying speed and position. The velocity update equation of particles is shown in Equation 11.

$$v_i(m+1) = v_i(m) + c_1 \times rand_1 \times \left(pb_i(m) - x_i(m)\right) + c_2 \times rand_2 \times \left(gb(m) - x_i(m)\right) \tag{11}$$

In Equation 11, i represents a particle, c_1 and c_2 are acceleration constants for the individual particle and particle swarm. $pb_i(m)$ and $gb(m)$ are the individual best and global best values at iteration m.

The particle position depends on the updated velocity and the previous position. The position update equation is shown in Equation 12.

$$x_i(m+1) = x_i(m) + v_i(m+1) \tag{12}$$

In Equation 12, $x_i(m)$ represents the position of particle i at iteration m.

Through the velocity and position update equations, individual and global best values are continuously updated and exchanged, and the optimal solution is updated accordingly. When data is highly complex, PSO computation increases, and search performance decreases. To improve PSO performance, the study introduces the Evaporation Constant (EC) to simplify particle design, obtaining the EC-PSO algorithm. The operational workflow of EC-PSO is illustrated in Figure 5.

In Figure 5, the EC-PSO algorithm workflow mainly completes parameter optimization by calculating and evaluating particle fitness and positions. Particles are first randomly initialized and checked against the termination condition. If the condition is satisfied, the result is output. If not, particle velocities and positions are updated, and fitness is calculated. The global best position is continuously updated, and the evaporation constant updates individual best positions. Individual and global best solutions are compared, and the optimal solution is updated. These steps repeat until the termination condition is satisfied, and the optimal solution is output. In the PSO algorithm, the search range and convergence speed of the particles are usually balanced by the dynamic inertia weight.

The formula of the velocity correction of the particle after the adjustment of the inertia weight is shown in Equation 13.

$$v_i(m+1)' = w \times v_i(m+1) \tag{13}$$

In Equation 13, $v_i(m+1)$ represents the velocity of particle i at iteration $m+1$, and w is the inertia factor. After introducing the evaporation constant, the particle position update equation in PSO is improved. The position-update equation based on the evaporation constant is given by Equation 14.

$$P_i = \begin{cases} TP_i(t), f(X_i(t)) \geq Tf(P_i(t)) \\ X_i(t), f(X_i(t)) < Tf(P_i(t)) \end{cases} \tag{14}$$

In Equation 14, T represents the evaporation constant, $f(X_i(t))$ represents particle fitness, and $f(P_i(t))$ represents the particle best fitness. By searching for the best fit value, the algorithm can adapt to the dynamic environment quickly. The formula for calculating the best fitness value is shown in Equation 15.

$$\begin{bmatrix} F_j(i+1) \\ x_j^{P_{best}} \end{bmatrix} = \begin{cases} \begin{bmatrix} \rho F_j(i) \\ x_j^{P_{best}} \end{bmatrix}, if\ \eta_{j+1} \geq \rho F_j(i) \\ \begin{bmatrix} \eta_{j+1} \\ x_j(i+1) \end{bmatrix}, if\ \eta_{j+1} < \rho F_j(i) \end{cases} \tag{15}$$

In Equation 15, ρ is the common evaporation constant of all particles, which is used to enlarge the current best fitness value and control the sensitivity of the algorithm to environmental changes, $\rho > 1$. F indicates the current best fit value, $x_j(i+1)$ indicates particle j is position at the current iteration, $x_j^{P_{best}}$ indicates the optimal position of the particle. η_{j+1} indicates the fitness value of the $j+1$-th particle, The formula for η_{j+1} is shown in Equation 16.

$$\eta_{j+1} = J\left(x_j(i+1)\right) \tag{16}$$

In Equation 16, J is the fitness value of the third particle in the second iteration. In Equation 16, J denotes the fitness value of the j-th particle during the i-th iteration.

After the evaporation constant is optimized, the PSO algorithm uses the particle positions to represent the controller's gain coefficient values, and the optimal parameters are determined by the fitness value size, i.e., whether the minimum fitness value is found.

Optimizing PSO with the evaporation constant enhances the computation speed of PSO. Using the optimized EC-PSO, STA-ASMC is improved to construct the motor speed regulation model named EPS-ASMC. The speed regulation process of EPS-ASMC is shown in Figure 6.

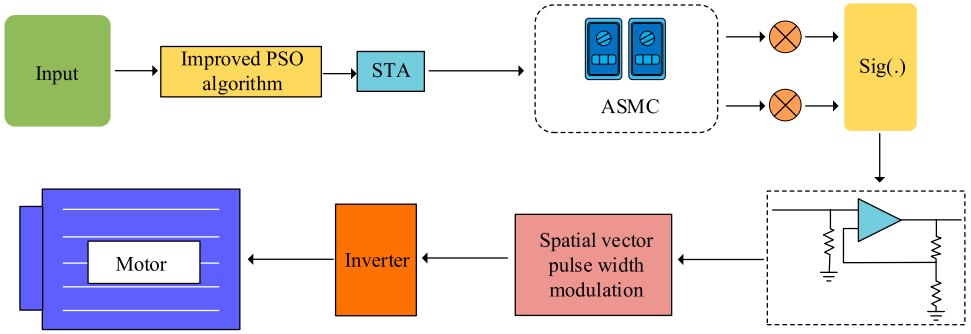

FIGURE 6
Speed regulation process of EPS-ASMC.

TABLE 1 Experimental parameter settings.

Number of particles	Symbol	Value
Number of particles	N	10
Iterations	N_{iter}	800
Evaporation constant	$[\rho_1,\rho_1]$	[1/0.85,1/0.999]
Stator phase resistance	R	2.875Ω
d-axis inductor and q-axis inductor	$L_d = L_q$	8.5 mH
Number of motor poles	p_n	4
Damping coefficient	B	0.008$N{\cdot}m{\cdot}s$
Torque constant	K_t	1.05$N{\cdot}m$
Moment of inertia	J	0.003 $kg{\cdot}m^2$
Synovial surface coefficient	k	200
Error derivative weight coefficient	q	300

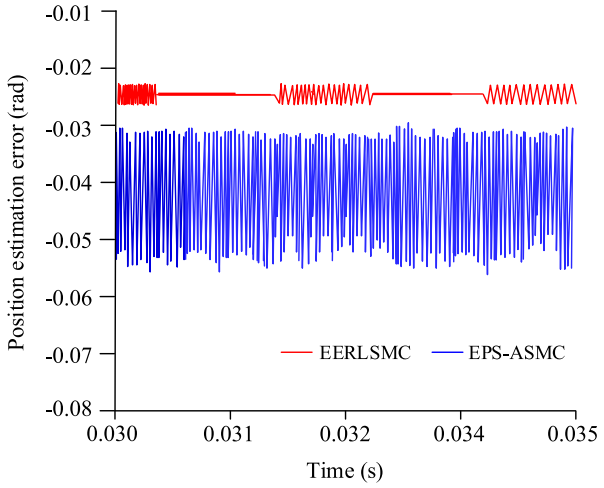

FIGURE 7
Rotor position estimation error comparison.

As shown in Figure 6, the EPS-ASMC speed regulation process first transmits motor state and position information to the current conversion module for data conversion. EC-PSO tunes the controller's parameters. STA adjusts the sliding mode gain coefficient and calculates the SMC rate for speed regulation. Then, an adaptive filter with an adaptive gain is designed to smooth the output information. The information is transmitted to the modulation signal generation module to produce signals, which are then fed into the three-phase inverter for conversion and subsequently used to control the motor drive speed.

4 Validation of the automatic motor speed regulation model combining STA and ASMC

4.1 Performance validation of the automatic motor speed regulation model

To verify the control performance of the model, simulations were conducted to evaluate the EPS-ASMC model. The experiments used a Permanent Magnet Synchronous Motor (PMSM) as an example and were implemented in MATLAB/Simulink. A motor speed regulation model was built in Simulink, and PMSM parameters were input into Simulink. Based on the motor control module library and the voltage and mechanical equations of the PMSM in the d-q coordinate system, motor states were simulated. Multiple simulations were performed under different speed and load conditions, and the resulting data were imported into the MATLAB workspace for visualization. The motor parameters and algorithm parameters used in the experiments are shown in Table 1.

Based on the parameters, the simulation model was built in Simulink for the experiments. To better evaluate model performance, the Enhanced Exponential Reaching Law Sliding Mode Controller (EERLSMC) was used for comparison. The experiments used a step size of 4×10^{-7}, a load of 5 Nm, and a rotor speed of 1,500 r/min. The study employs the Enhanced Exponential Reaching Law Sliding Mode Controller (EERLSMC), which demonstrates superior vibration suppression performance, to conduct a comparative analysis with the model, thereby providing a more intuitive and thorough evaluation of the EPS-ASMC model's control performance (Gudey and Naguboina, 2021). After 0.030 s,

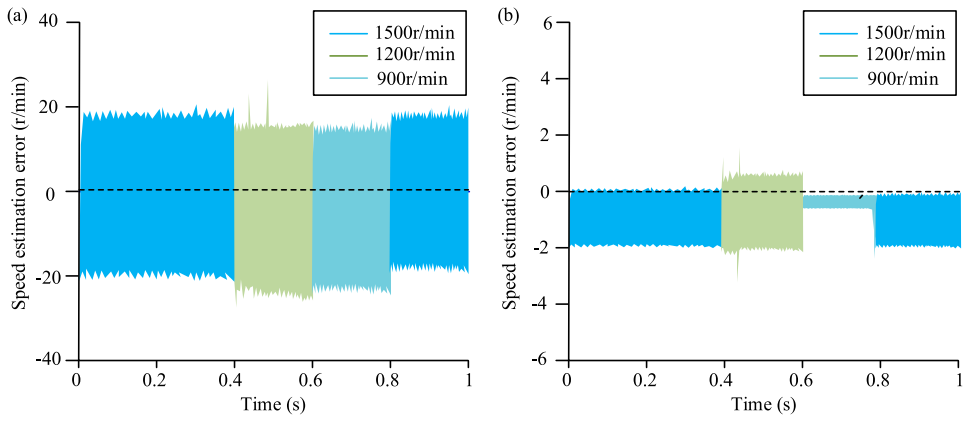

FIGURE 8
Comparison of speed estimation errors. **(a)** The speed estimation error of EERLSMC **(b)** The speed estimation error of RPS-ASMC.

both controllers reach a steady state. The rotor position estimation error in 0.030s–0.035s is compared between the two controllers to analyze their steady-state control performance. The comparison results are shown in Figure 7.

As shown in Figure 7, the rotor position estimation error of EERLSMC fluctuates between [−0.058rad, −0.031rad] at a control speed of 1,500 r/min, while the rotor position estimation error of EPS-ASMC remains within [−0.026 rad, −0.023 rad] at the same control speed, demonstrating lower errors compared to the EERLSMC model. Additionally, compared to EERLSMC, the position estimation error curve of the proposed model is more stable, with a smaller chattering amplitude, indicating better stability. This is attributed to the use of the super-spiral algorithm to improve SMC in the proposed model, which adjusts the convergence coefficient and sliding mode surface coefficient to reduce chattering. To further analyze model performance, the rotor speed was suddenly changed from 1,500 r/min to 1,200 r/min and 900 r/min at 0.4 s and 0.6 s under constant load. The speed estimation errors of the two methods were compared, as shown in Figure 8.

In Figure 8a, the EERLSMC speed estimation error remained between −25 r/min and 25 r/min, which was relatively large. In Figure 8b, the EPS-ASMC model controlled the speed estimation error within −2 r/min to 0 r/min at 1,500 r/min. When the speed suddenly changed to 1,200 r/min, the EPS-ASMC model reached a stable state within 0.05 s, demonstrating better control performance. Overall, the EPS-ASMC model outperformed the comparison model in convergence speed, stability, and accuracy.

4.2 Speed regulation evaluation of the EPS-ASMC model

Based on the performance verification, the EPS-ASMC model was further evaluated for speed regulation effectiveness. The same simulation environment was used, and static experiments were conducted to assess static speed regulation performance. Two sets of experiments were designed with zero load: the first at 1,200 r/min and the second at 1800 r/min. The results are shown in Figure 9.

As shown in Figure 9a, at 1,200 r/min, the estimated speed curve of EPS-ASMC closely matched the actual speed, and the maximum speed estimation error remained within 2.12 r/min. In Figure 9b, at 1800 r/min, the estimated speed curve matched the actual speed even more closely, with a maximum estimation error below 2.10 r/min, indicating low estimation error. Following static experiments, three dynamic experiments were conducted to analyze dynamic speed regulation. All experiments were under no load. In Experiment 1, the speed was increased from 600 to 900 and then to 1,200. In Experiment 2, it decreased from 1,200 to 900 and then to 600. In Experiment 3, the speed was set to 1,800, then to 1,500, and finally to 1,200. All speeds are in r/min. The acceleration and deceleration results of Experiments 1 and 2 are shown in Figure 10.

As shown in Figure 10a, in Experiment 1, the EPS-ASMC model converged to 900 r/min in 0.70 s during the first acceleration, showing fast convergence. During the second acceleration, convergence occurred in 2.34 s. In both cases, the model reached the target speed within 2.50 s, confirming its fast convergence. The estimated speed curve closely matched the actual speed, demonstrating effective regulation. In Figure 10b, during the two decelerations of Experiment 2, convergence times were 0.90 s and 1.45 s, further confirming the model's dynamic regulation performance. To further analyze the dynamic speed regulation performance of the model, the study compares it with two motor speed control models: the Improved Sparrow Search Algorithm-Proportional-Integral-Derivative Controller (ISSA-PID) and the Extended State Observer-Sliding Mode Control (ESO-SMC) (Zhang et al., 2024; Fei and Liu, 2023). The experimental analysis focused on current waveforms across the d-axis and q-axis in Experiment 1, with evaluations of maximum speed estimation errors and overshoot measurements for each model. The comprehensive assessment results are presented in Figure 11.

As shown in Figure 11a, during the acceleration test in Experiment 1, the EPS-ASMC model demonstrated stable current fluctuations along the d-axis during abrupt speed changes, maintaining near-constant values. The q-axis current fluctuations remained within ±0.10A, exhibiting high stability. Figure 11b reveals that the EPS-ASMC model achieved a maximum speed estimation error of 5.77% in Experiment 1, 2.15% lower than the MC-CMAC model, 1.67% less than the ISSA-PID model, and 0.93% smaller than

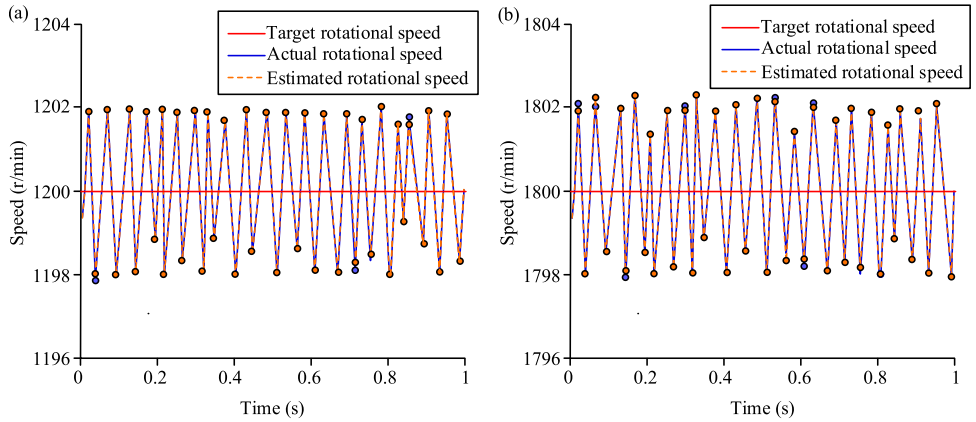

FIGURE 9
Static speed regulation analysis of EPS-ASMC. **(a)** The speed variation curve at 1,200r/min **(b)** The speed variation curve at 1,800r/min.

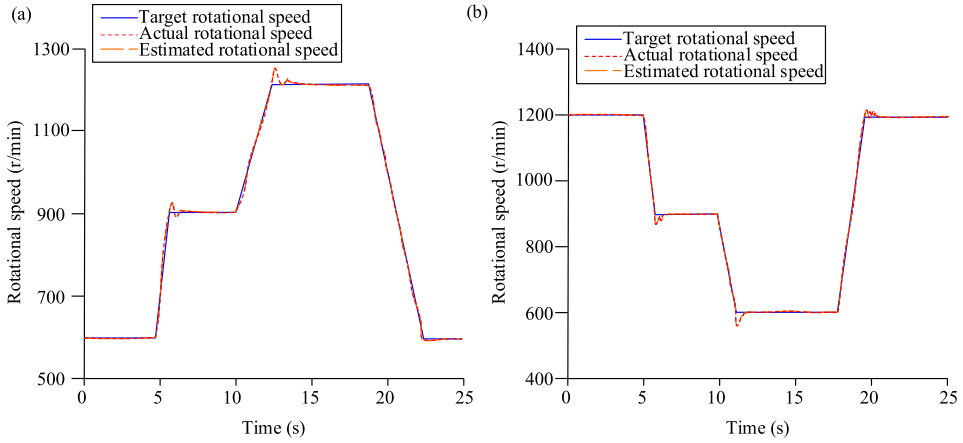

FIGURE 10
Speed variation curves during acceleration and deceleration. **(a)** The rotational speed variation curve of Experiment 1 **(b)** The rotational speed variation curve of Experiment 2.

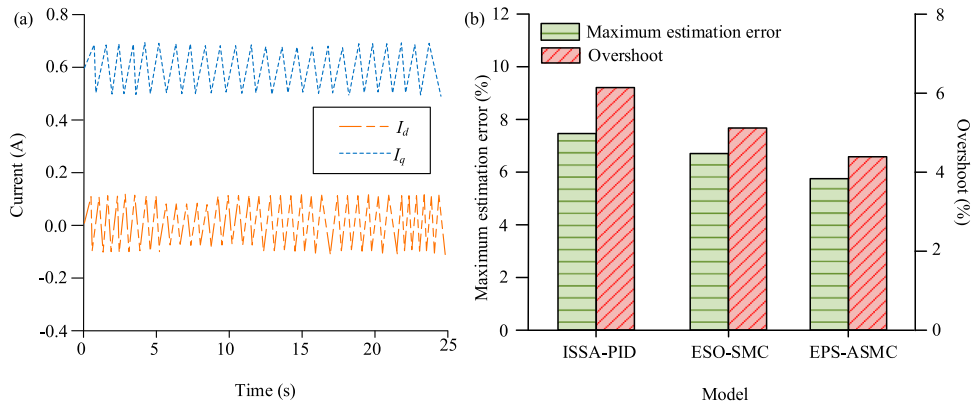

FIGURE 11
Analysis of the speed regulation effect of the model. **(a)** The current variation curve of EPS-ASMC in Experiment 1urrent variation curve of Experiment 1 **(b)** Comparison of overshoot and maximum estimation error of each model in Experiment 1.

the ESO-FxTSMC model. These results not only meet the standard requirement of <8.00% error but also demonstrate superior performance in motor speed control. Additionally, the EPS-ASMC model exhibited a 4.44% overshoot rate in Experiment 1, which was significantly lower than those of its comparison models, further highlighting its enhanced control capabilities. This achievement is attributed to the research's innovative model design, which employs adaptive gain coefficients for control to effectively mitigate phase lag. The system further achieves rapid, vibration-free convergence by adjusting real-time sliding-mode gains via STA. In contrast, both ISSA-PID and ESO-SMC models lack adaptive mechanisms, resulting in delayed dynamic response and limited observation accuracy under high-frequency disturbances. In conclusion, the proposed EPS-ASMC model demonstrates optimized speed regulation performance, enabling more precise automated speed control for motor systems.

5 Summary

To address the current issues in motor speed regulation, such as susceptibility to disturbances and high computational demand, this study proposed an automated motor speed regulation model combining STA and ASMC. The model designed an adaptive controller using SMC and adaptive gain, applied STA to suppress controller chattering, and optimized controller parameters using the EC-PSO algorithm. Ultimately, the EPS-ASMC automated speed regulation model was developed to control motor speed. Experimental results showed that at a control speed of 1,500 r/min, the rotor position estimation error of EPS-ASMC remained essentially stable within −0.026 rad to −0.023 rad. The position estimation error curve was smooth with reduced chattering amplitude. In dynamic experiments, the d-axis current fluctuation remained stable during sudden speed changes, and the q-axis current fluctuation stayed within ±0.10 A, indicating high stability. Additionally, the maximum speed estimation error of EPS-ASMC was 5.77% in Experiment 1% and 7.68% in Experiment 2, and in all three experiments, the maximum error remained below the 8.00% standard, meeting the speed regulation requirements in the motor field. Overall, the EPS-ASMC model demonstrated superior speed regulation performance, providing stable and efficient automated motor speed control. Although the proposed model exhibited high accuracy and rapid response, its performance under varying system parameters and external disturbances was not thoroughly investigated. Future work will explore the speed regulation performance of the model under different disturbances and continuously improve its speed and accuracy to enhance its applicability.

Data availability statement

The original contributions presented in the study are included in the article/supplementary material, further inquiries can be directed to the corresponding author.

Author contributions

YZ: Writing – original draft, Writing – review and editing, Conceptualization, Data curation. YL: Writing – original draft, Writing – review and editing, Formal Analysis, Investigation, Methodology.

Funding

The author(s) declared that financial support was not received for this work and/or its publication.

Conflict of interest

The author(s) declared that this work was conducted in the absence of any commercial or financial relationships that could be construed as a potential conflict of interest.

Generative AI statement

The author(s) declared that generative AI was not used in the creation of this manuscript.

Any alternative text (alt text) provided alongside figures in this article has been generated by Frontiers with the support of artificial intelligence and reasonable efforts have been made to ensure accuracy, including review by the authors wherever possible. If you identify any issues, please contact us.

Publisher's note

References

Bao, H., Zhu, H., and Liu, D. (2024). Improved SSA-RBF neural network-based dynamic 3-D trajectory tracking model predictive control of autonomous underwater vehicles with external disturbances. *Optim. Control Appl. Methods* 45 (1), 138–162. doi:10.1002/oca.3050

Chen, Z., Xiao, F., Chen, W. C. Z., and Tang, W. (2023). An improved model predictive direct speed control with synchronous prediction and weight factor optimization for PMSM application. *J. Electr. Eng. and Technol.* 18 (6), 4257–4268. doi:10.1007/s42835-023-01486-z

Cheng, Y., Yang, W., Xu, W., and Zhong, S. (2025). Impulsive effects on delayed fractional-order neural networks: sliding mode control-based fixed-time synchronization analysis. *Nonlinear Dyn.* 113 (13), 16571–16592. doi:10.1007/s11071-025-10955-1

Deng, C., Zheng, H., Gong, L., Zhang, R., and Wang, M. (2025). An improved local RBF collocation method for 3D excavation deformation based on direct method and mapping technique. *CMES-COMPUTER Model. Eng. and Sci.* 142 (2), 2147–2172. doi:10.32604/cmes.2025.059750

Fang, W., Yang, Z., Jia, W. P., Wang, G., and Jia, P. (2023). Displacement sensorless control of a bearingless induction motor based on hybrid flux estimation. *Int. Journal Green Energy* 20 (11/15), 1423–1433. doi:10.1080/15435075.2022.2155966

Fei, J., and Liu, L. (2023). Fuzzy neural super-twisting sliding-mode control of active power filter using nonlinear extended state observer. *IEEE Trans. Syst. Man, Cybern. Syst.* 54 (1), 457–470. doi:10.1109/tsmc.2023.3310593

Ge, W., and Wang, X. (2025). PSO–LSTM–Markov coupled photovoltaic power prediction based on sunny, cloudy and rainy weather. *J. Electr. Eng. and Technol.* 20 (2), 935–945. doi:10.1007/s42835-024-02051-y

Geromel, J. C., Nunes, E. V. L., and Hsu, L. (2024). Lmi-based robust multivariable super-twisting algorithm design. *IEEE Trans. Automatic Control* 69 (7), 4844–4850. doi:10.1109/tac.2024.3358235

Gudey, S. K., and Naguboina, V. K. (2021). Enhanced exponential reaching law-based sliding mode control of ShAPF in an EDS. *J. Eng. Res.* 18 (1), 52–61. doi:10.53540//tjervol18iss1pp52-61

Hill, J., Fahimi, F., Kang, C. K., and Aono, H. (2025). Adaptive discrete-time sliding mode control applied to the pitch motion of a micro air vehicle with flapping wings. *J. Bionic Eng.* 22 (2), 585–595. doi:10.1007/s42235-025-00658-z

Huang, H., Tang, G., Chen, H., Wang, J., Han, L., and Xie, D. (2025). Full-order sliding mode control of underwater flexible manipulators with echo state network disturbance compensation. *Trans. Can. Soc. Mech. Eng.* 49 (2), 249–263. doi:10.1139/tcsme-2023-0209

Jiang, J., Zhang, H., Jin, D., Wang, A., and Liu, L. (2024). Disturbance observer based non-singular fast terminal sliding mode control of permanent magnet synchronous motors. *J. Power Electron.* 24 (2), 249–257. doi:10.1007/s43236-023-00725-w

Li, M., Zhu, J., Liu, Q., Liao, H., and Zang, K. (2025). A novel model predictive current control for fault tolerant permanent magnet vernier rim-driven motor based on improved sector selection. *J. Electr. Eng. and Technol.* 20 (1), 703–712. doi:10.1007/s42835-024-02020-5

Liu, M., Xu, N., Wang, H., Zong, G., Zhao, X., and Li, L. (2025a). Hierarchical non-singular terminal sliding mode control for constrained under-actuated nonlinear systems against sensor faults. *Nonlinear Dyn.* 113 (13), 16913–16929. doi:10.1007/s11071-025-11011-8

Liu, Z., Gong, X., and Fei, J. (2025b). Nonsingular fast terminal sliding mode control of DC–DC buck converter using fuzzy neural network and disturbance observer. *Nonlinear Dyn.* 113 (11), 13389–13414. doi:10.1007/s11071-024-10857-8

Mapui, A., Arzoo Jamal, M., and Mukhopadhyay, S. (2025). Fixed/Predefined-time stability and designing of terminal sliding mode control of impulsive dynamical systems. *Int. J. Syst. Sci.* 56 (1), 139–156. doi:10.1080/00207721.2024.2388809

Musarrat, M. N., Fekih, A., Ashib RahmanMd, Md., and Muttaqi, R. I. K. M. (2024). An event triggered sliding mode control-based fault ride-through scheme to improve the transient stability of wind energy systems. *IEEE Trans. Industry Appl.* 60 (1), 876–886. doi:10.1109/TIA.2023.3328851

Rauth, S. S., Kastha, D., and Bajpai, P. (2024). A sensorless control strategy for automatic start-up and grid-synchronization of doubly fed induction generator in wind energy conversion system. *Int. Journal Circuit Theory Applications* 52 (4), 1733–1753. doi:10.1002/cta.3843

Yang, H., Xu, J., Ma, S., and Zhang, Y. (2025). Synchronous SVM-based model predictive flux control of induction motor drives with fast phase synchronization. *IEEE Trans. Power Electron.* 40 (5), 6413–6422. doi:10.1109/tpel.2025.3525804

Zaghba, L., Borni, A., Benbitour, M. K., and Fezzani, A. (2025). Improving photovoltaic energy harvesting systems with hybrid fuzzy logic-PI MPPT optimized by PSO under normal and partial shading conditions. *Electr. Eng.* 107 (4), 4897–4919. doi:10.1007/s00202-024-02800-2

Zhang, H., Zhang, Y., and Zhu, Y. W. X. (2023). Robust deadbeat predictive current control of induction motor drives with improved steady state performance. *IET Power Electron.* 16 (8), 1281–1292. doi:10.1049/pel2.12469

Zhang, M., Xu, C., Li, L., Wang, Z., and Zong, X. (2024). Optimization of PID controller for stepper motor speed control system based on improved sparrow search algorithm. *Proc. Institution Mech. Eng. Part C J. Mech. Eng. Sci.* 238 (19), 9397–9411. doi:10.1177/09544062241261268

Zhao, T., Zhu, J., Liu, Q., Wu, J., and Cai, Y. (2025). Sensorless control of fault-tolerant permanent magnet vernier rim-driven motor based on improved model reference adaptive system. *J. Power Electron.* 25 (4), 687–697. doi:10.1007/s43236-024-00920-3